# Early Permian magmatism in Briançonnais terranes : Truzzo granite and Roffna rhyolite (eastern Penninic nappes, Swiss and Italian Alps)

Autor(en): **Marquer, Didier / Challandes, Nathalie / Schaltegger, Urs**

Objekttyp: **Article**

Zeitschrift: **Schweizerische mineralogische und petrographische Mitteilungen = Bulletin suisse de minéralogie et pétrographie**

Band (Jahr): **78 (1998)**

Heft 3

PDF erstellt am: **19.05.2024**

Persistenter Link: https://doi.org/10.5169/seals-59297

SCHWEIZ. MINERAL. PETROGR. MITT. 78, 397–414, 1998

# Early Permian magmatism in Briançonnais terranes: Truzzo granite and Roffna rhyolite (eastern Penninic nappes, Swiss and Italian Alps)

by *Didier Marquer*[1], *Nathalie Challandes*[1] and *Urs Schaltegger*[2]

**Abstract**

In the internal part of the Central Alps, heterogeneous Tertiary deformation of basement nappes led to large weakly deformed domains. This is where studies of pre-Alpine magmatism can be performed. The Truzzo granite and the Roffna rhyolite, which are part of the Penninic Tambo and Suretta nappes, respectively, are shallow-seated intrusions in old polycyclic basement rocks. Petrographical, geochemical and isotopic similarities suggest that Truzzo granite and Roffna rhyolite are part of the same post-orogenic magmatic event. Furthermore, U–Pb systematics on single zircon give a $^{206}Pb/^{238}U$ age of 268.0 ± 0.4 Ma for the Truzzo granite and a $^{206}Pb/^{238}U$ age of 268.3 ± 0.6 Ma for the Roffna rhyolite. These intrusions were derived from the mixing of crustal and mantle sources, as indicated by the isotopic results and the occurrence of different types of xenoliths.

The proximity of these intrusions becomes apparent in an Early Permian reconstruction of the Briançonnais terrane. They might have had their origin in upwelling asthenospheric mantle, related to lithospheric thinning at the site of the future Jurassic rifting and opening of the Liguro-Piemontais ocean.

*Keywords:* granites, U–Pb ages, zircons, Early Permian magmatism, Penninic nappes, Central Alps.

## Introduction

Orogens normally comprise imbricated crystalline terranes which have to be integrated in pre-collisional paleogeographical reconstructions. The main problem for studying such strongly deformed basement is to distinguish between structures that pre-date the most recent orogenic cycle, in order to get information about pre-collisional structures, petrology and geochemistry of these rocks. Very heterogeneous deformation, in some places within the Alpine nappe pile, has allowed the preservation of metamorphic and magmatic relics (MARQUER, 1991; BIINO et al., 1997), which can be used to reconstruct the lithological composition, geochemistry and geochronology of pre-Alpine basement and intrusive rocks. In the case of intrusive rocks, it is necessary to determine primary mineralogical compositions, magmatic textures and geochemical characteristics in order to constrain their geodynamic setting in the earlier, pre-Alpine (Variscan) orogenic cycle.

The Swiss Alps are usually divided into three broad domains from north to south: (i) an external, Helvetic domain, (ii) an internal part, the Penninic zone and (iii) the South-Alpine and Austroalpine units, the latter exposed on top of the Alpine edifice (COWARD and DIETRICH, 1989). Basement rocks in the Helvetic domain and the South- and Austro-Alpine units did not undergo strong penetrative Alpine deformation, facilitating the petrological and geochemical studies of pre-Alpine structures and magmatism in these areas. On the contrary, the Penninic zone represents the strongly deformed internal parts of the Alpine mountain belt, the result of collision between the European plate in the north and the Adriatic plate in the south, with a series of microcontinents in between, one of them being the Briançonnais terrane. The Penninic domain consists of imbricate stacks of sedimentary cover and basement slices with a complex nappe geometry as the result of both thrust tectonics and post-nappe refolding (Fig. 1) (SCHMID et al., 1990; SCHREURS, 1993;

[1] Geological Institute, 11, rue E. Argand, CH-2007 Neuchâtel, Switzerland. <didier.marquer@geol.unine.ch>
[2] Department of Earth Sciences, ETH-Zentrum, Sonneggstrasse 5, CH-8092 Zürich, Switzerland.

PFIFFNER et al., 1990; MARQUER et al., 1996). Our investigations focus on the basement rocks of the upper Penninic Tambo and Suretta nappes in the eastern internal Swiss Alps, which belong to the Briançonnais paleogeographic domain (Fig. 1) (TRÜMPY, 1980). The tectonic framework of the frontal part of the Suretta nappe and of the Tambo nappe has been recently described by MARQUER et al. (1996) and BAUDIN et al. (1993) (Fig. 2). One of the main results from these recent studies is that Tertiary deformation of the basement rocks was strongly heterogeneous, leading to the preservation of undeformed lenticular domains surrounded by mylonites at a broad range of scales. Petrological and geochronological studies of pre-Alpine intrusives can therefore be concentrated on these areas of weak Alpine deformation.

Two granitoid bodies, the mostly effusive to subvolcanic Roffna rhyolite in the northern part of the Suretta nappe (GRÜNENFELDER, 1956; MARQUER et al., 1996) and the Truzzo granite in the southern part of the Tambo nappe (WEBER, 1966; MARQUER, 1991) were investigated (Fig. 2). Previously published Variscan ages for these granitoids show strong discrepancies: for the Truzzo granite, a 339 ± 70 Ma U–Pb age for zircon (GRÜNENFELDER in WEBER, 1966) and a 293 ± 14 Ma Rb–Sr whole rock age (GULSON, 1973) were measured. For the Roffna rhyolite an intrusion age around 350 Ma (U–Pb zircon) was suggested by HANSON et al. (1969). Based on new mapping, petrological and isotopic studies, we propose a close genetic link between these two intrusives. Precise intrusion ages and geochemical characteristics permit their integration in reconstructions of the Pre-Alpine setting of the Briançonnais terrane. The role and significance of this type of magmatic activity will be discussed with respect to late and post-Variscan tectonics prior to the opening of the Tethys ocean.

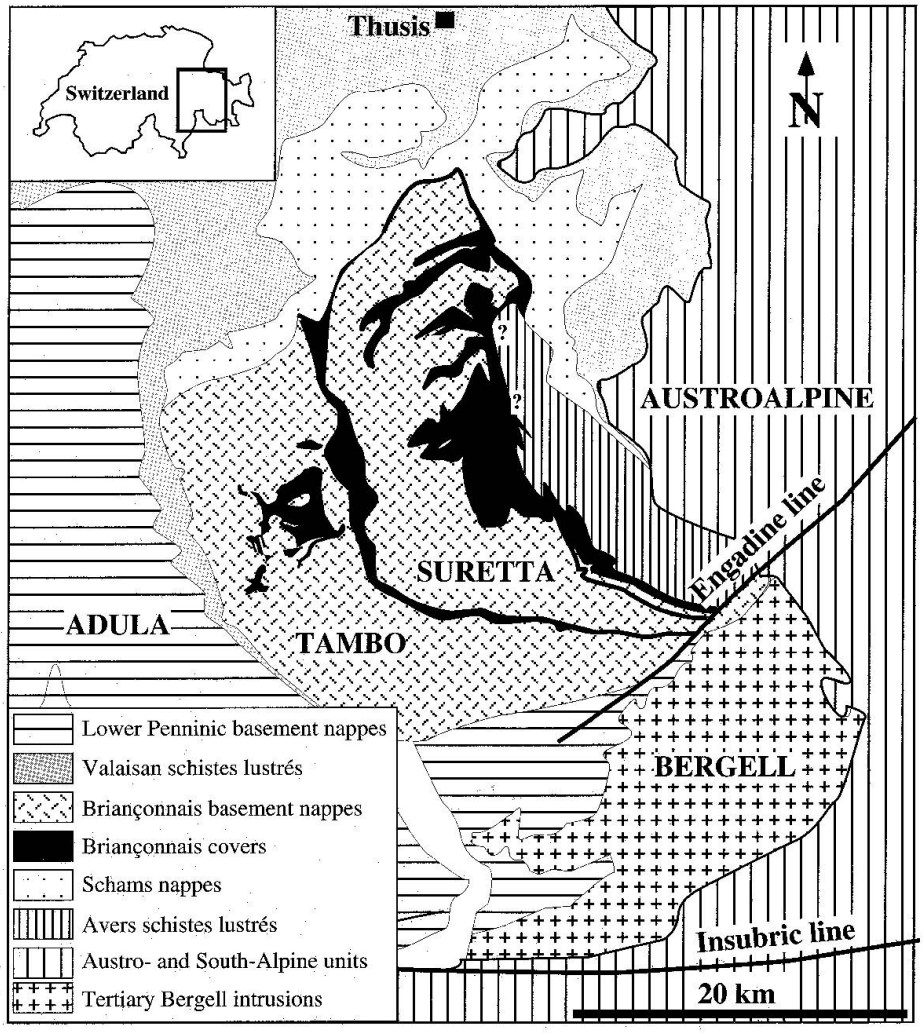


*Fig. 1* Location of the Tambo and Suretta nappes on a simplified geological map of the eastern part of the Central Alps.

## Geological setting

The Tambo and Suretta nappes form two ca. 3.5 km thick crystalline slivers, mainly composed of old crystalline basement (Fig. 2). The polymetamorphic basement is essentially composed of metapelites and metagreywackes including lenses of mafic rocks (amphibolites), porphyritic orthogneisses and local migmatites (STAUB, 1916; WILHELM, 1921; GANSSER, 1937; GRÜNENFELDER, 1956; ZURFLÜH, 1961; STROHBACH, 1965; SCHAEREN, 1974). The study of metamorphism and deformation in the mafic lenses has led to the recognition of two distinct metamorphic events, a pre-Alpine HP-HT and an Alpine HP-LT one (BIINO et al., 1997; NUSSBAUM et al., 1998). In the Suretta nappe, a late Variscan subvolcanic intrusion is located in the frontal part, the so-called Roffna rhyolite (Roffna porphyry; GRÜNENFELDER, 1956; STREIFF et al., 1976; MARQUER et al., 1996; Fig. 2). The Tambo basement was intruded by the Truzzo granite in the south (WEBER, 1966; BLANC, 1965; GULSON, 1973; MARQUER, 1991) (Fig. 2).

The autochthonous cover of the Tambo and Suretta nappes is composed of a volcanoclastic and a reduced carbonate series. The Permo-Triassic volcanoclastic cover (BAUDIN et al., 1993), including some effusive metatuffs in the Splügen area, lies unconformably on the basement of both the Tambo and the Suretta nappes (Fig. 2). Conglomerates at the base of the stratigraphic pile show lithological similarities to the classic "Verrucano" facies and pass progressively into more and more quartzitic formations. The volcanoclastic succession is covered by a pure quartzite layer, only present in the Suretta nappe and probably Scythian in age. The Mesozoic calcareous cover above this volcanic and epiclastic series directly overlies the basement rocks in a few places (BAUDIN et al., 1995). This mesozoic cover shows sedimentary sequences typical of the Briançonnais terranes (BAUDIN et al., 1995).

Alpine deformations led to the development of a complex pattern of shear zones that isolate lenses of weakly deformed basement rocks (WEBER, 1966; MARQUER, 1991; BAUDIN et al., 1993; MARQUER et al., 1994, 1996). Only the two first main deformations were responsible for large scale shear zones that show substantial petrological and geochemical modification of the initial rocks (MARQUER and PEUCAT, 1994; CHALLANDES, 1996). Chemical mass transfer related to Alpine heterogeneous deformation have been recorded in high-strain zones but only subordinate chemical changes have occurred in weakly deformed rocks (MARQUER, 1989; MARQUER and PEUCAT, 1994). To avoid textural and chemical perturbations related to Alpine deformations in high-strain zones, only samples from weakly deformed zones were collected for the following study.

## Petrology and intrusive structures of granitoids

### TRUZZO GRANITE

The Truzzo granite is a E-W-elongated intrusive body located in the southern part of the Tambo nappe (Fig. 2). The granite cross-cuts different lithologic units such as older orthogneisses, banded migmatites and amphibolites, which were previously deformed under high grade conditions (Fig. 2). Primary magmatic contacts with the surrounding gneissic rocks are sub-vertical and show characteristics of syn-intrusive deformation of the granitoid, such as preferred orientation of large K-feldspar porphyroclasts and enclaves (MARQUER, 1991). Mafic magmatic enclaves and basement xenoliths (orthogneisses, migmatitic gneisses) are present in the whole body of the porphyritic granite as well as in one granite sample (HTC 7) from the southern contact with migmatitic rocks, where some restitic enclaves occur. The granite underwent strong Alpine deformation in some places (BLANC, 1965; WEBER, 1966). In weakly deformed domains, the granite appears as an originally isotropic and homogeneous body of porphyritic granite with large K-feldspar porphyroclasts, oligoclase, brown biotite and primary muscovite.

The top of the granite intrusion is mainly composed of alternating layers of a K-feldspar bearing porphyritic facies and an isogranular leucocratic facies. The layering probably corresponds to intrusions of leucocratic granite sills into the porphyritic granite. The main body of leucocratic granite is of small size (1 $km^2$) and is located in the core of the porphyritic granite (tunnel of Cimaganda oil pipeline, San Bernardino). This leucocratic granite is K-feldspar rich and contains primary muscovite and scarce pink garnet. Isolated small stocks of Truzzo granite occur within the banded migmatite gneiss and amphibolite in the southern part of the Tambo nappe (Piz Pizasc, Piz Matter, Val di Liro; Fig. 2). The granite is commonly overlain by a thin sequence of polymetamorphic basement rocks, particularly in the southeastern part of the area, close to the Permo-Triassic cover. The Truzzo granite is interpreted as an intrusion with several apophyses emplaced at shallow depth in the upper crust (WEBER, 1966).

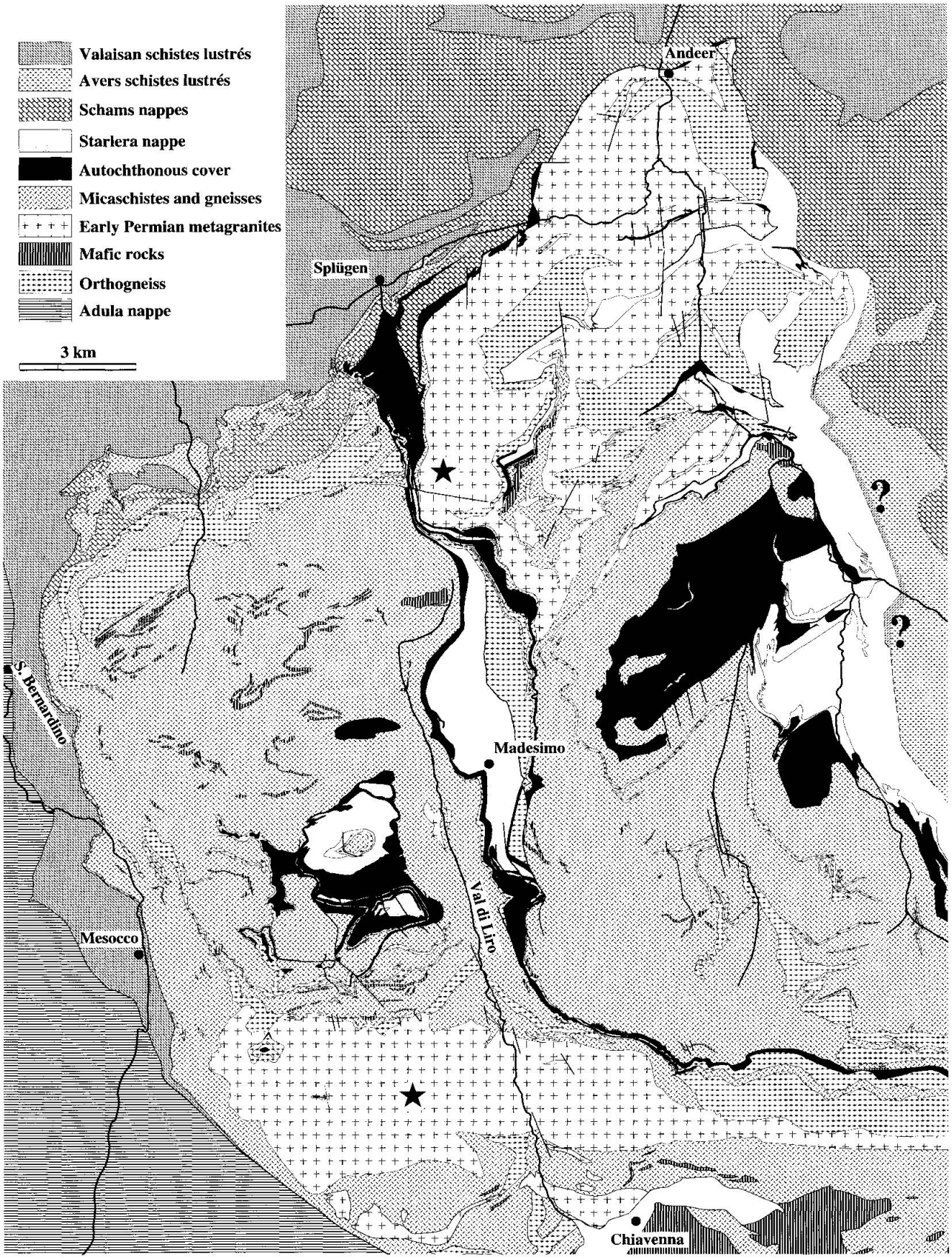


*Fig. 2* Geological map of the Tambo and Suretta nappes. Geological boundaries of the Valais schistes lustrés and Schams nappes are from SCHREURS (1993). The contact between Avers – autochthonous cover of Suretta is not well-defined on this map (question marks). Asterisks correspond to the location of U–Pb analysed samples in the Truzzo granite and Roffna rhyolite (Tab. 3).

## ROFFNA RHYOLITE

In the frontal part of the Suretta nappe, GRÜNENFELDER (1956) described a large body of crystalline rocks he termed "Roffnaporphyr". Recent mapping and petrographic studies resulted in a better separation of the Roffna rhyolite from older orthogneisses in this area (Fig. 2). The Roffna rhyolite has been interpreted as a high-level intrusion of subvolcanic nature (GRÜNENFELDER, 1956; MILNES and SCHMUTZ, 1978), or alternatively, suggested to be a caldera filling at the top of the nappe (DALLA TORRE, 1991). The amphibolites, banded migmatites and old orthogneisses are

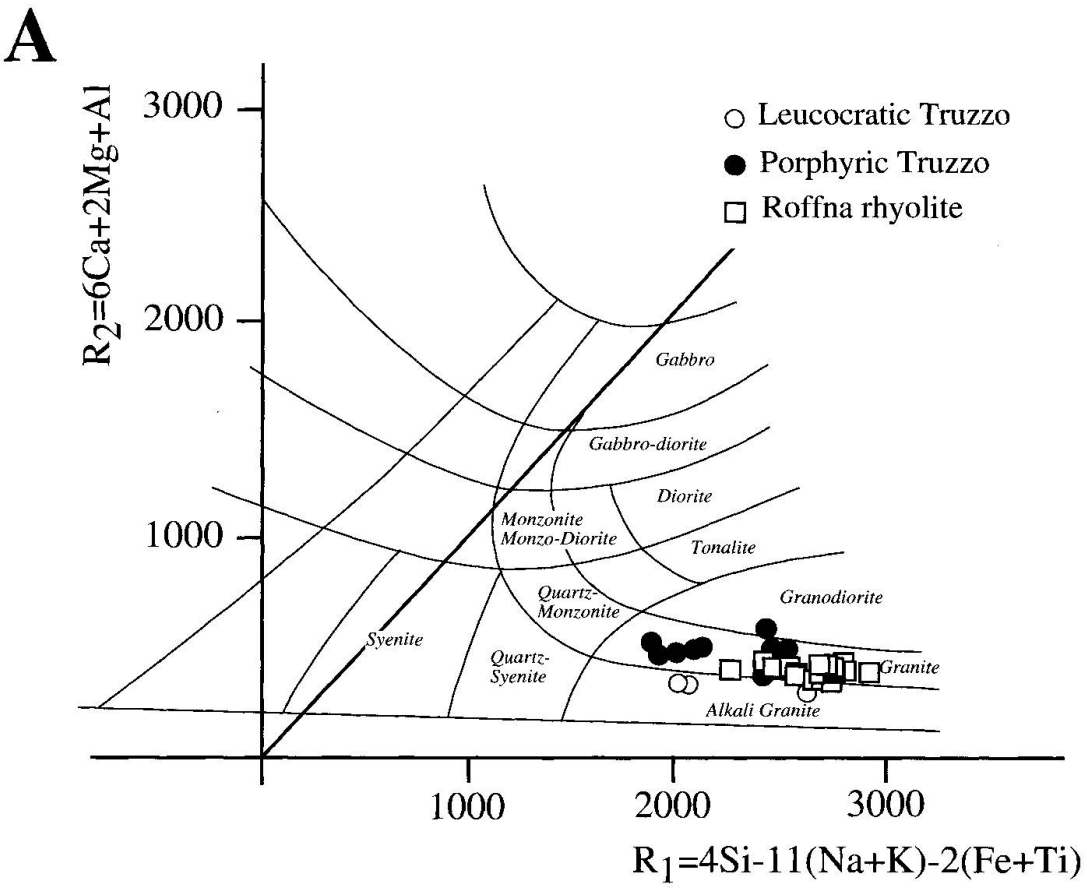


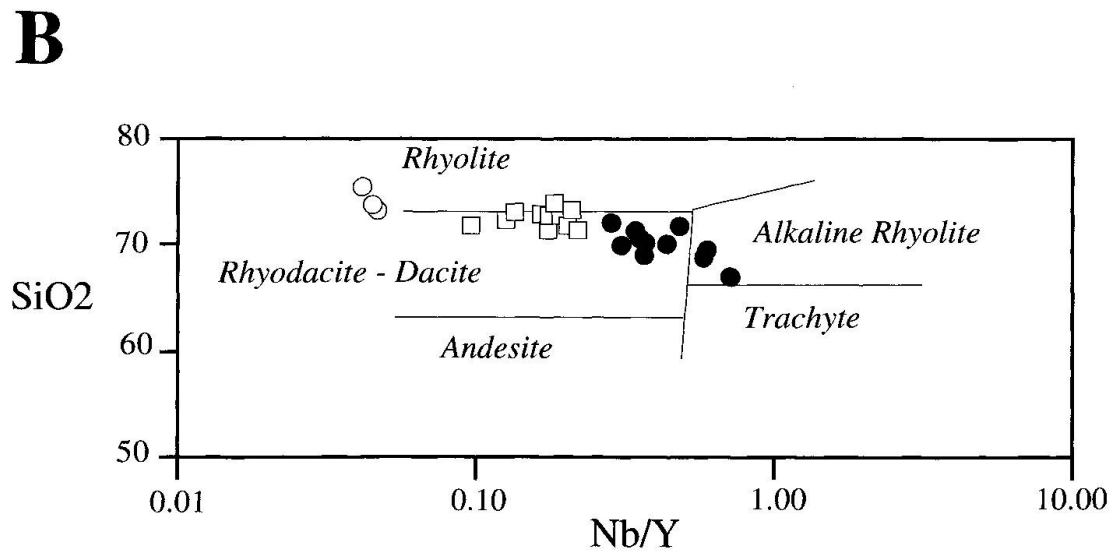


*Fig. 3* Nomenclature of the Truzzo and Roffna intrusive rocks. A: R1-R2 diagram after de LA ROCHE et al. (1980). B: $SiO_2$/(Nb/Y) after WINCHESTER and FLOYD (1977).

clearly cross-cut by the Roffna rhyolite at several locations at the base and center of the Suretta nappe (Fig. 2). These intrusive relationships between the foliated basement and the Roffna rhyolite demonstrate that the basement rocks were strongly deformed under high grade metamorphic conditions before Lower Permian (NUSSBAUM et al., 1998). The Roffna rhyolite hosts abundant enclaves of three main types: xenoliths of various basement gneisses, leucocratic felsic enclaves and a few small mafic microgranular enclaves. The latter contain corroded quartz grains originating from the rhyolite, which argues for magmatic mingling between acid and basic magmas during emplacement. All enclaves show a distinct preferred orientation of magmatic origin. The formation of K-feldspar phenocrysts along contacts and the partial assimilation of orthogneiss xenoliths suggest high-temperature emplacement of the rhyolite at upper crustal levels. At the base of the frontal part of the Suretta nappe (Splügen pass area), the monocyclic volcanosedimentary cover is mainly composed of metatuffs and cinerites strongly affected by Alpine deformation (autochthonous cover, Fig. 2). In weakly deformed samples, the Roffna rhyolite contains large phenocrysts of partly bi-pyramidal or corroded quartz, microcline, oligoclase, brown biotite and rare pink garnet within a homogeneous microcrystalline matrix. Normally, the fine-grained matrix had recrystallised during Alpine metamorphism. In some places, close to the contact with the old orthogneisses or around xenoliths of old orthogneisses, the Roffna rhyolite shows an enrichment of large K-feldspar phenocrysts. In that case, the old orthogneissic xenoliths show diffusive boundaries and partial assimilation which might suggest a high-temperature emplacement of the rhyolite at upper crustal levels.

## Geochemistry

### TRUZZO GRANITE

The samples of the porphyritic granite lie in the granite field of the R1-R2 diagram of de LA ROCHE et al. (1980; Fig. 3A, Black dots). The leucocratic garnet-muscovite-bearing granite, on the other hand, is located in the alkali granite field of the same diagram (Fig. 3A, white dots), while it plots in the rhyolite field in a $SiO_2$–Nb/Y diagram (WINCHESTER and FLOYD, 1977) with very low Nb/Y ratios (Fig. 3B, white dots). The alkaline tendency of this leucocratic granite is probably due to the low amounts of CaO (Fig. 3A). The low concentrations of CaO, $Fe_2O_3$, MgO, $TiO_2$, the minor element chemistry, and the occurrence of either acmite or normative corundum in the CIPW norm are responsible for the peralkaline or peraluminous affinity, respectively, of these granitic rocks (Fig. 4, white and black dots). This position, as well as the scatter along the peralkaline-peraluminous transition, is due to slight variations of the (Na + K)/Al ratio and is typical of low-calcium granites.

### ROFFNA RHYOLITE

The Roffna rhyolite samples plot in the granite field of the R1-R2 diagram (Fig. 3A, white squares) and along the boundary between rhyolite and rhyodacite fields in the $SiO_2$–Nb/Y diagram (Fig. 3B, white squares). All samples correspond to peraluminous granite and are located in the field of continental collision granites (CCG) in figure 4. They show a homogeneous composition with $SiO_2$ concentrations ranging between 71 and 74% (Fig. 5). Despite the slight scattering of some mobile elements, probably related to Alpine deformation (mainly for $K_2O$, $Na_2O$, CaO, Ba, Rb and Sr), the Roffna samples show a similar magmatic trend for major and minor elements in Harker diagrams as those of the Truzzo samples (Fig. 5). The Roffna samples define a compositional range that seems to be part of the trend between leucocratic and porphyric granite of the Truzzo intrusion (Fig. 5). Their compositional variation in a $K_2O/SiO_2$ diagram emphasises the affinity with classical alkaline or high-K calc-alkaline suites (Fig. 5).

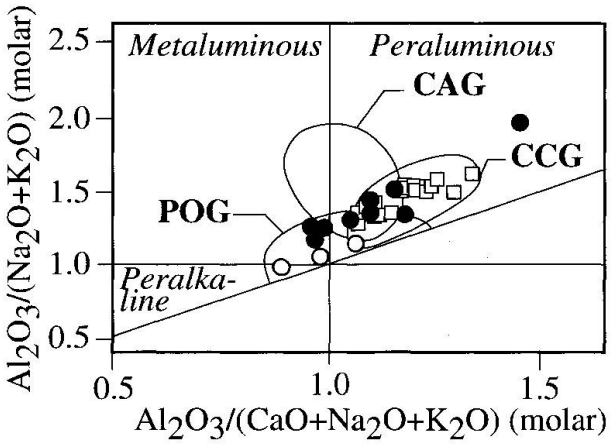


*Fig. 4* Distribution of the Truzzo and Roffna samples with respect to the Shand's index modified after MANIAR and PICCOLI (1989). CAG: continental arc granitoids; CCG: continental collision granitoids; POG: post-orogenic granitoids. Same symbols as in figure 3.

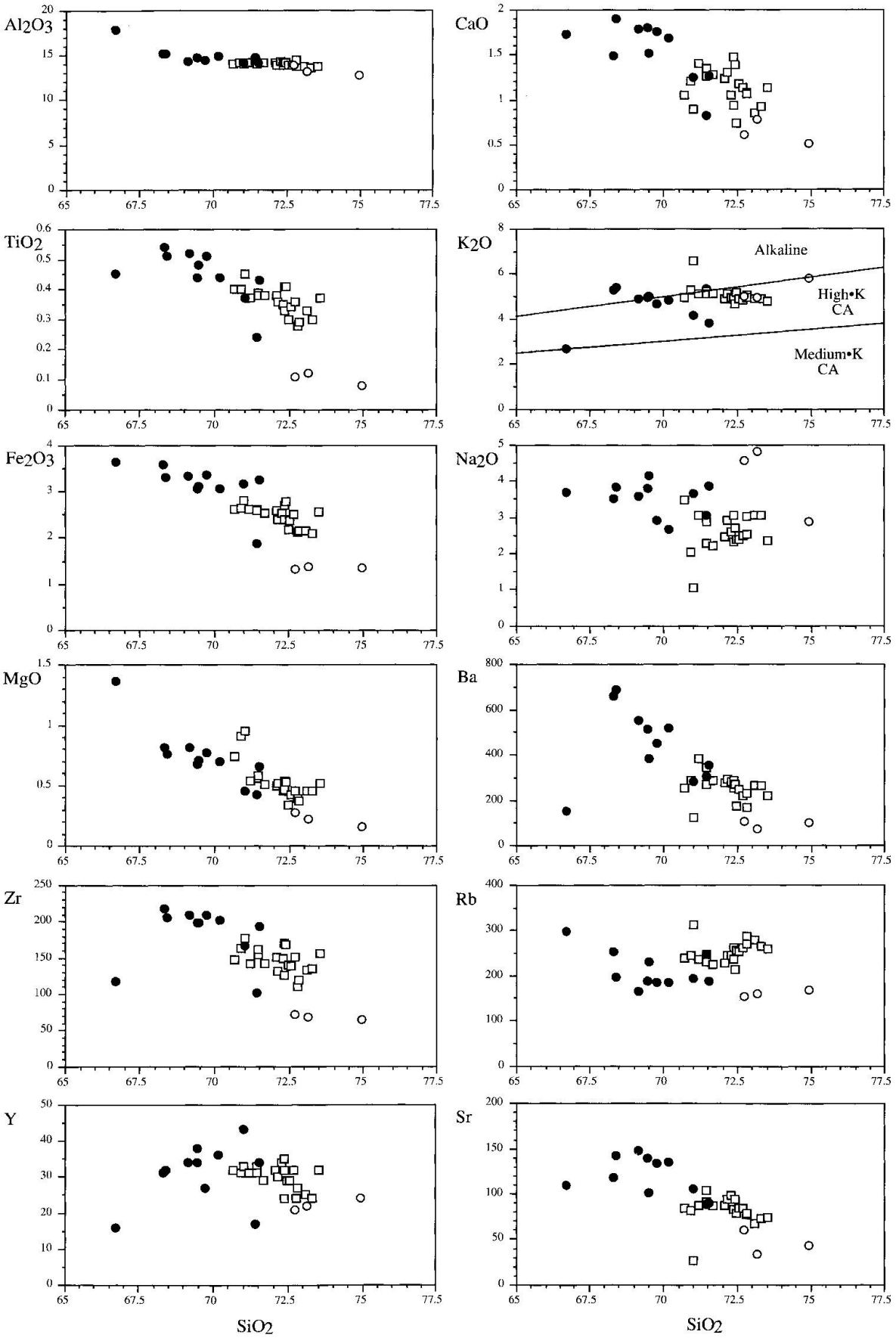


*Fig. 5* Some major and minor elements illustrating the magmatic trends in Harker's diagrams. Same symbols as in figure 3. The high-K and medium-K fields are defined after PECCERILLO and TAYLOR (1976).

*Tab. 1* Chemical analyses of the Truzzo granite and the Roffna rhyolite. Same symbols as in figure 3. X and Y correspond to the Swiss topographic coordinates.

| Symboles | □ | □ | □ | □ | □ | □ | □ | □ | □ | □ | □ | □ | □ | □ | □ | □ | □ | □ | □ | □ | □ |
|---|---|---|---|---|---|---|---|---|---|---|---|---|---|---|---|---|---|---|---|---|---|
| Samples | RC3 | RC4 | RC5 | RC9 | RC19 | RC20 | RC24 | RC28 | RC29 | RC30 | RC31 | RC32 | RC33 | RC38 | RC39 | RC44 | RC46 | RSZ1a | RSZ1z | RSZ2a | RSZ3c |
| $SiO_2$ | 72.55 | 72.28 | 72.47 | 72.68 | 71.45 | 72.36 | 71.00 | 72.82 | 71.68 | 72.07 | 72.39 | 70.90 | 73.52 | 71.18 | 72.14 | 70.67 | 71.44 | 72.36 | 73.29 | 72.79 | 73.08 |
| $TiO_2$ | 0.34 | 0.35 | 0.30 | 0.36 | 0.38 | 0.41 | 0.45 | 0.29 | 0.38 | 0.38 | 0.41 | 0.40 | 0.37 | 0.37 | 0.36 | 0.40 | 0.39 | 0.33 | 0.30 | 0.28 | 0.33 |
| $Al_2O_3$ | 13.89 | 14.28 | 14.14 | 13.90 | 14.00 | 14.09 | 14.01 | 14.37 | 14.10 | 14.11 | 14.10 | 14.18 | 13.71 | 14.11 | 13.84 | 14.01 | 14.14 | 13.90 | 13.54 | 13.75 | 13.75 |
| $Fe_2O_3$ | 0.23 | 0.67 | 0.71 | 0.58 | 0.46 | 0.59 | 1.57 | 0.49 | 0.75 | 0.92 | 0.28 | 0.85 | 1.40 | 0.85 | 0.90 | 1.19 | 1.28 | 1.06 | | 0.01 | |
| FeO | 1.93 | 1.69 | 1.33 | 1.74 | 1.91 | 1.90 | 1.13 | 1.49 | 1.62 | 1.50 | 2.26 | 1.61 | 1.05 | 1.60 | 1.40 | 1.29 | 1.20 | 1.22 | | 1.91 | |
| $Fe_2O_3$* | 2.37 | 2.55 | 2.19 | 2.51 | 2.58 | 2.70 | 2.82 | 2.14 | 2.55 | 2.59 | 2.79 | 2.64 | 2.57 | 2.63 | 2.40 | 2.62 | 2.61 | 2.41 | 2.10 | 2.13 | 2.16 |
| MnO | 0.04 | 0.04 | 0.03 | 0.04 | 0.04 | 0.04 | 0.03 | 0.04 | 0.05 | 0.04 | 0.04 | 0.03 | 0.05 | 0.04 | 0.04 | 0.04 | 0.03 | 0.03 | 0.04 | 0.03 | 0.04 |
| MgO | 0.42 | 0.46 | 0.34 | 0.45 | 0.58 | 0.54 | 0.95 | 0.37 | 0.51 | 0.50 | 0.53 | 0.91 | 0.52 | 0.54 | 0.52 | 0.74 | 0.56 | 0.47 | 0.45 | 0.39 | 0.45 |
| CaO | 1.18 | 1.05 | 0.74 | 1.14 | 1.34 | 1.47 | 0.90 | 1.07 | 1.27 | 1.24 | 1.39 | 1.20 | 1.14 | 1.40 | 1.30 | 1.05 | 1.26 | 0.94 | 0.92 | 1.08 | 0.85 |
| $Na_2O$ | 2.40 | 2.59 | 2.40 | 2.49 | 2.29 | 2.31 | 1.03 | 2.52 | 2.20 | 2.44 | 2.70 | 2.02 | 2.35 | 3.06 | 2.90 | 3.49 | 2.89 | 3.04 | 3.04 | 3.01 | 3.05 |
| $K_2O$ | 4.88 | 4.97 | 5.16 | 4.86 | 5.12 | 4.95 | 6.56 | 4.96 | 5.13 | 4.88 | 4.67 | 5.27 | 4.75 | 5.13 | 5.09 | 4.97 | 5.25 | 4.90 | 4.90 | 5.04 | 4.91 |
| $P_2O_5$ | 0.15 | 0.15 | 0.15 | 0.15 | 0.13 | 0.14 | 0.15 | 0.17 | 0.15 | 0.14 | 0.15 | 0.14 | 0.16 | 0.13 | 0.14 | 0.13 | 0.13 | 0.14 | 0.16 | 0.14 | 0.16 |
| $H_2O$ | 1.03 | 1.08 | 1.25 | 1.21 | 1.45 | 1.27 | 2.22 | 1.15 | 1.23 | 1.27 | 1.18 | 1.72 | 1.07 | 0.97 | 1.02 | 1.90 | 1.19 | 1.14 | 0.79 | 0.92 | 0.84 |
| Sum: | 99.04 | 99.61 | 99.02 | 99.60 | 99.15 | 100.07 | 100.00 | 99.74 | 99.07 | 99.49 | 100.10 | 99.23 | 100.09 | 99.38 | 99.65 | 99.88 | 99.76 | 99.53 | 99.53 | 99.35 | 99.62 |
| Rb | 252 | 244 | 256 | 261 | 231 | 237 | 311 | 286 | 224 | 226 | 214 | 243 | 259 | 236 | 244 | 240 | 246 | 261 | 264 | 271 | 277 |
| Sr | 85 | 98 | 79 | 85 | 104 | 83 | 27 | 79 | 88 | 87 | 95 | 82 | 75 | 88 | 94 | 84 | 92 | 83 | 73 | 77 | 67 |
| Nb | 5 | 7 | 4 | 6 | 3 | 6 | 6 | 6 | 6 | 4 | 7 | 7 | 6 | 6 | 4 | 1 | 5 | 6 | 13 | 3 | 14 |
| Zr | 139 | 150 | 141 | 151 | 161 | 170 | 178 | 119 | 142 | 151 | 169 | 164 | 157 | 142 | 131 | 148 | 154 | 127 | 135 | 111 | 133 |
| Y | 29 | 34 | 29 | 32 | 31 | 32 | 33 | 27 | 29 | 32 | 35 | 31 | 32 | 31 | 30 | 32 | 33 | 24 | 24 | 24 | 25 |
| U | 4 | 4 | 2 | 5 | 5 | 6 | 2 | 4 | 4 | 3 | 5 | 3 | 6 | 1 | 1 | 0 | 3 | 1 | | 1 | |
| Th | 12 | 15 | 12 | 14 | 14 | 15 | 19 | 10 | 11 | 13 | 16 | 15 | 15 | 11 | 10 | 10 | 11 | 10 | 14 | 6 | 16 |
| Pb | 29 | 18 | 23 | 27 | 30 | 31 | 19 | 26 | 31 | 28 | 34 | 74 | 30 | 31 | 19 | 18 | 23 | 17 | 31 | 29 | 30 |
| Ga | 17 | 18 | 18 | 18 | 17 | 18 | 18 | 18 | 18 | 17 | 18 | 17 | 18 | 13 | 14 | 14 | 14 | 15 | | 13 | |
| Zn | 40 | 40 | 35 | 47 | 42 | 46 | 31 | 39 | 45 | 42 | 44 | 40 | 47 | 41 | 41 | 42 | 43 | 45 | 39 | 40 | 42 |
| Cu | 0 | 0 | 0 | 0 | 0 | 0 | 0 | 0 | 0 | 0 | 0 | 0 | 0 | 0 | 0 | 0 | 0 | 0 | 4 | 0 | 5 |
| Ni | 5 | 6 | 5 | 6 | 4 | 5 | 6 | 4 | 4 | 3 | 4 | 4 | 6 | 1 | 1 | 2 | 3 | 2 | 4 | 1 | 5 |
| Co | 30 | 36 | 36 | 37 | 34 | 32 | 30 | 39 | 40 | 32 | 43 | 35 | 40 | 33 | 35 | 27 | 28 | 37 | | 44 | |
| Cr | 12 | 9 | 5 | 10 | 8 | 13 | 11 | 4 | 14 | 9 | 11 | 8 | 12 | 10 | 8 | 10 | 11 | 8 | 14 | 7 | 22 |
| V | 19 | 25 | 17 | 23 | 22 | 21 | 36 | 16 | 21 | 23 | 24 | 26 | 21 | 26 | 22 | 29 | 22 | 21 | 21 | 18 | 18 |
| Ce | 57 | 57 | 49 | 54 | 53 | 59 | 59 | 42 | 54 | 52 | 63 | 60 | 53 | 61 | 57 | 69 | 58 | 48 | | 45 | |
| Nd | 23 | 25 | 19 | 22 | 16 | 21 | 28 | 14 | 21 | 22 | 23 | 23 | 23 | 24 | 26 | 24 | 23 | 18 | | 20 | |
| Ba | 246 | 284 | 177 | 218 | 272 | 290 | 124 | 170 | 288 | 274 | 271 | 289 | 220 | 382 | 292 | 253 | 346 | 255 | 267 | 231 | 265 |
| La | 27 | 29 | 21 | 19 | 23 | 27 | 26 | 14 | 20 | 21 | 23 | 18 | 21 | 31 | 33 | 34 | 30 | 23 | | 23 | |
| S | 48 | 46 | 41 | 57 | 77 | 61 | 72 | 45 | 51 | 61 | 139 | 153 | 54 | 47 | 0 | 66 | 0 | 0 | | 0 | |
| Coordinate X | 745.85 | 745.85 | 745.90 | 753.15 | 752.65 | 752.75 | 753.97 | 749.55 | 750.15 | 750.40 | 751.65 | 751.70 | 753.15 | 746.30 | 746.25 | 748.90 | 748.10 | 746.00 | 746.00 | 746.00 | 746.00 |
| Coordinate Y | 152.35 | 152.30 | 152.25 | 157.50 | 161.65 | 161.50 | 163.75 | 159.45 | 159.15 | 159.10 | 160.25 | 160.20 | 157.50 | 151.85 | 152.10 | 158.50 | 158.30 | 152.25 | 152.25 | 152.25 | 152.25 |

*Tab. 1* (cont.).

| Symboles | ○ | ○ | ○ | ● | ● | ● | ● | ● | ● | ● | ● | ● | ● | ● |
|---|---|---|---|---|---|---|---|---|---|---|---|---|---|---|
| Samples | HTC5 | TC1a | TC2a | HTC1 | HTC2 | HTC3 | HTC4 | HTC6 | HTC7 | TC3a | TC4a | TC5a | TC6a | TC7a |
| $SiO_2$ | 74.94 | 73.14 | 72.71 | 71.01 | 68.40 | 69.15 | 70.18 | 71.42 | 66.71 | 71.52 | 69.48 | 69.45 | 68.32 | 69.75 |
| $TiO_2$ | 0.08 | 0.12 | 0.11 | 0.37 | 0.51 | 0.52 | 0.44 | 0.24 | 0.45 | 0.43 | 0.48 | 0.44 | 0.54 | 0.51 |
| $Al_2O_3$ | 12.80 | 13.15 | 13.84 | 14.17 | 15.12 | 14.29 | 14.85 | 14.69 | 17.82 | 14.22 | 14.70 | 14.68 | 15.08 | 14.43 |
| $Fe_2O_3$ | 0.90 | 0.41 | 0.47 | 2.75 | 2.29 | 0.69 | 1.45 | 0.39 | 0.82 | 2.15 | 0.53 | 0.85 | 0.78 | 1.63 |
| FeO | 0.41 | 0.87 | 0.76 | 0.37 | 0.91 | 2.40 | 1.46 | 1.34 | 2.55 | 1.01 | 2.34 | 2.00 | 2.54 | 1.56 |
| $Fe_2O_3$* | 1.36 | 1.38 | 1.31 | 3.16 | 3.30 | 3.35 | 3.07 | 1.88 | 3.65 | 3.27 | 3.13 | 3.07 | 3.60 | 3.36 |
| MnO | 0.06 | 0.06 | 0.06 | 0.02 | 0.04 | 0.04 | 0.04 | 0.03 | 0.09 | 0.03 | 0.05 | 0.03 | 0.03 | 0.04 |
| MgO | 0.16 | 0.22 | 0.28 | 0.46 | 0.76 | 0.81 | 0.70 | 0.42 | 1.37 | 0.66 | 0.71 | 0.68 | 0.82 | 0.77 |
| CaO | 0.52 | 0.78 | 0.61 | 1.25 | 1.90 | 1.79 | 1.69 | 0.82 | 1.73 | 1.26 | 1.51 | 1.80 | 1.49 | 1.76 |
| $Na_2O$ | 2.88 | 4.82 | 4.57 | 3.64 | 3.84 | 3.60 | 2.68 | 3.06 | 3.68 | 3.88 | 4.16 | 3.78 | 3.51 | 2.91 |
| $K_2O$ | 5.78 | 4.94 | 4.99 | 4.17 | 5.41 | 4.89 | 4.86 | 5.36 | 2.71 | 3.83 | 5.03 | 4.92 | 5.29 | 4.67 |
| $P_2O_5$ | 0.12 | 0.13 | 0.12 | 0.13 | 0.18 | 0.18 | 0.13 | 0.28 | 0.20 | 0.09 | 0.17 | 0.17 | 0.33 | 0.14 |
| $H_2O$ | 0.40 | 1.02 | 1.23 | 0.65 | 0.60 | 0.89 | 0.59 | 1.20 | 1.88 | 0.72 | 0.62 | 0.63 | 1.04 | 0.66 |
| Sum: | 99.05 | 99.66 | 99.75 | 98.99 | 99.96 | 99.25 | 99.07 | 99.25 | 100.01 | 99.80 | 99.78 | 99.43 | 99.77 | 98.83 |
| Rb | 169 | 161 | 153 | 194 | 196 | 166 | 185 | 246 | 297 | 189 | 231 | 189 | 254 | 185 |
| Sr | 44 | 34 | 61 | 106 | 143 | 148 | 135 | 89 | 110 | 90 | 102 | 140 | 119 | 134 |
| Nb | 1 | 1 | 1 | 15 | 12 | 21 | 13 | 5 | 12 | 17 | 12 | 13 | 19 | 12 |
| Zr | 65 | 68 | 72 | 167 | 206 | 210 | 202 | 101 | 117 | 193 | 198 | 198 | 218 | 210 |
| Y | 24 | 22 | 21 | 43 | 32 | 34 | 36 | 17 | 16 | 34 | 38 | 34 | 31 | 27 |
| U | 0 | 2 | 0 | 4 | 0 | 1 | 2 | 0 | 4 | 2 | 3 | 1 | 2 | 1 |
| Th | 1 | 2 | 2 | 18 | 16 | 16 | 17 | 0 | 12 | 16 | 17 | 16 | 15 | 17 |
| Pb | 40 | 32 | 28 | 18 | 34 | 37 | 36 | 43 | 24 | 25 | 33 | 36 | 34 | 0 |
| Ga | 14 | 16 | 15 | 21 | 16 | 20 | 19 | 18 | 29 | 20 | 18 | 19 | 22 | 8 |
| Zn | 17 | 15 | 13 | 75 | 48 | 61 | 59 | 53 | 123 | 105 | 50 | 53 | 62 | 25 |
| Cu | 0 | 0 | 0 | 0 | 0 | 0 | 0 | 7 | 18 | 0 | 0 | 0 | 0 | 0 |
| Ni | 6 | 5 | 5 | 9 | 5 | 9 | 10 | 9 | 18 | 8 | 9 | 9 | 9 | 0 |
| Co | 31 | 24 | 37 | 24 | 29 | 33 | 37 | 48 | 44 | 45 | 38 | 42 | 31 | 27 |
| Cr | 0 | 0 | 1 | 11 | 10 | 15 | 14 | 12 | 43 | 13 | 11 | 13 | 12 | 0 |
| V | 2 | 3 | 1 | 28 | 41 | 43 | 34 | 16 | 49 | 37 | 37 | 38 | 44 | 33 |
| Ce | 0 | 17 | 13 | 61 | 81 | 79 | 83 | 51 | 61 | 76 | 80 | 77 | 77 | 86 |
| Nd | 3 | 5 | 7 | 34 | 37 | 31 | 41 | 18 | 22 | 36 | 43 | 42 | 35 | 37 |
| Ba | 100 | 74 | 108 | 285 | 688 | 555 | 521 | 307 | 151 | 356 | 382 | 514 | 658 | 453 |
| La | 5 | 7 | 8 | 27 | 32 | 33 | 32 | 20 | 32 | 33 | 36 | 34 | 31 | 32 |
| S | 0 | 0 | 0 | 8 | 0 | 0 | 0 | 0 | 0 | 0 | 0 | 0 | 0 | 0 |
| Coordinate X | 745.00 | 747.30 | 747.30 | 745.00 | 745.00 | 745.00 | 745.00 | 742.75 | 742.75 | 743.85 | 748.95 | 744.95 | 744.80 | 744.80 |
| Coordinate Y | 136.00 | 136.80 | 136.80 | 136.00 | 136.00 | 136.00 | 136.00 | 133.25 | 133.25 | 136.40 | 133.00 | 136.10 | 136.20 | 136.20 |

Due to strong assimilation of basement xenoliths, sample HTC 7 (66.71% $SiO_2$, Tab. 1; black dot on Fig. 4; weight: 5 kg), containing 10–20% xenoliths, is not representative. Nevertheless, it is important to consider this sample because it represents the most contaminated geochemical end-member. It gives an idea on the magnitude of crustal contamination effects in shifting points in figures 3 and 4 with respect to the other samples free of xenoliths.

## Geochronology

### Rb–Sr

The age of intrusion of the Truzzo granite has so far been controversial: 339 ± 70 Ma ($^{207}Pb/^{206}Pb$ age, GRÜNENFELDER in WEBER 1966), 305 Ma (Rb–Sr whole rock age; JÄGER et al., 1969) or 293 ± 14 Ma (Rb–Sr whole rock age; GULSON, 1973). The previoulsy published Rb–Sr analyses of the Truzzo granite by GULSON (1973) and MARQUER et al. (1994) are given in table 2, for comparison with our new isotopic data of the Roffna rhyolite. The combined isotopic data yield a Rb–Sr reference line of 285 ± 22 Ma (Fig. 6) with a large MSWD value of 82, indicating post-crystallization disturbance of the Rb–Sr whole-rock system (Fig. 6, black dots). The age of the Roffna rhyolite, on the other hand, has previously been considered to be around 350 Ma ($^{207}Pb/^{206}Pb$ age of zircons; HANSON et al., 1969). Eleven samples of weakly deformed rhyolite were selected and yielded a reference line with an age approximate of 275 ± 100 Ma (MSWD = 197; Fig. 6, squares).

The Rb–Sr reference lines for weakly deformed samples from both lithologies give elevated errors much in excess of analytical scatter. The high MSWD values reflect effects of the Alpine metamorphism and deformation recorded by these granites (STEINITZ and JÄGER, 1981). It has

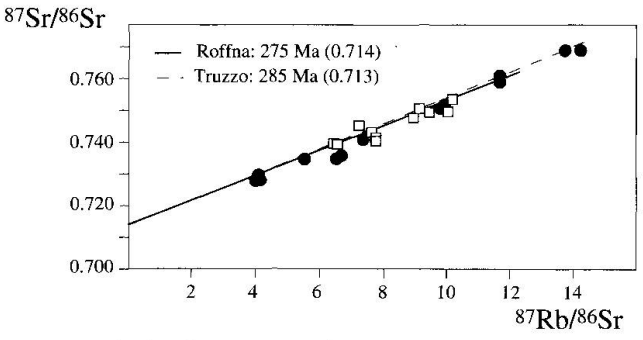


*Fig. 6* Rb–Sr diagram for the Truzzo and Roffna granitoids. Same symbols as in figure 3. See text for explanations.

*Tab. 2* Rb–Sr isotopic analyses of the Truzzo granite and the Roffna rhyolite. Analyses labelled G.xx were taken from GULSON (1973).

| | Rb ppm | Sr ppm | $^{87}Rb/^{86}Sr$ | $^{87}Sr/^{86}Sr$ |
|---|---|---|---|---|
| **Truzzo granite** | | | | |
| HTC2 | 196 | 143 | 3.97 | 0.73070 |
| HTC4 | 185 | 135 | 3.90 | 0.72928 |
| TC2a | 152 | 60.2 | 7.32 | 0.74256 |
| TC4a | 226 | 99.8 | 6.57 | 0.73775 |
| TC5a | 192 | 139 | 4.02 | 0.72940 |
| TC6a | 254 | 114 | 6.46 | 0.73625 |
| G.73.791 | 255 | 131 | 5.46 | 0.73650 |
| G.73.105/4 | 305 | 89.5 | 9.72 | 0.75200 |
| G.73.105/7 | 315 | 91.1 | 9.86 | 0.75340 |
| G.73.789 | 207 | 51.8 | 11.51 | 0.76270 |
| G.73.789/1 | 208 | 51.2 | 11.59 | 0.75970 |
| G.73.790 | 266 | 56.6 | 13.98 | 0.77060 |
| G.73.790/1 | 266 | 56.4 | 14.19 | 0.77070 |
| **Roffna rhyolite** | | | | |
| RC3 | 257 | 83.5 | 8.92 | 0.74752 |
| RC4 | 236 | 96.7 | 7.09 | 0.74597 |
| RC5 | 255 | 80.2 | 9.26 | 0.74900 |
| RC19 | 236 | 104.7 | 6.53 | 0.74125 |
| RC31 | 218 | 94.2 | 6.73 | 0.73925 |
| RC33 | 259 | 75.6 | 9.95 | 0.74971 |
| RC38 | 241 | 87.6 | 8.00 | 0.74161 |
| RC39 | 249 | 92.2 | 7.84 | 0.74390 |
| RC46 | 245 | 91.1 | 7.81 | 0.74144 |
| RSZ1a | 260 | 81.5 | 9.28 | 0.75107 |
| RSZ2a | 270 | 75.3 | 10.41 | 0.75489 |

to be pointed out, however, that these deviations are minor when compared to those from more intensely deformed rock portions, shifting Rb/Sr ratios to lower values in amphibolite-facies examples and to higher values in greenschist-facies examples (MARQUER and PEUCAT, 1994). The initial isotopic ratio for the Truzzo granite and the Roffna rhyolite are relatively high, 0.713 and 0.714 respectively, implying a significant continental component in the granitic rocks. It should be noted that all the samples underwent a similar degree of Alpine metamorphic overprint and deformation and show identical initial Sr isotopic ratios for both Roffna rhyolite and Truzzo granite (Fig. 6).

### U–Pb

To better constrain the emplacement age of both types, zircon populations were separated from representative samples of the Truzzo granite (TC5a) and the Roffna rhyolite (RC38) and analyzed for their Pb and U isotopic composition (Fig. 7 a and b; Tab. 3). These samples were chosen because they are located far from the intrusion boundaries and their chemical analyses are close

*Tab. 3* U–Pb analyses for the Truzzo granite and the Roffna rhyolite.

| Number | Description a) | Weight [mg] | n° of grains | Concentrations U [ppm] | Pb rad. [ppm] | Pb nonrad. [pg] | Th/U b) | Atomic ratios 206/204 c) | 206/238 d) | Error 2σ [%] | 207/235 d) | Error 2σ [%] | 207/206 d) | Error 2σ [%] | Apparent ages 206/238 | 207/235 | 207/206 | Error corr. |
|---|---|---|---|---|---|---|---|---|---|---|---|---|---|---|---|---|---|---|
| **Roffna rhyolite (RC38)** | | | | | | | | | | | | | | | | | | |
| 1 | spr, euh | 0.0103 | 6 | 672 | 34.5 | 7.2 | 0.13 | 3253 | 0.05423 | 0.34 | 0.4221 | 0.40 | 0.05645 | 0.17 | 340.4 | 357.5 | 470.3 | 0.91 |
| 2 | spr, euh | 0.0128 | 4 | 534.4 | 25.3 | 6.5 | 0.18 | 3248 | 0.04938 | 0.34 | 0.3704 | 0.41 | 0.05441 | 0.18 | 310.7 | 320.0 | 388.0 | 0.90 |
| 3 | lpr, clrls | 0.0093 | 8 | 675 | 30.4 | 14.7 | 0.16 | 1264 | 0.04736 | 0.34 | 0.3466 | 0.48 | 0.05308 | 0.30 | 298.3 | 302.2 | 332.2 | 0.78 |
| 4 | eq, brownish | 0.0070 | 5 | 512 | 36.9 | 6.3 | 0.17 | 2681 | 0.07535 | 0.34 | 0.6084 | 0.41 | 0.05856 | 0.20 | 468.3 | 482.6 | 550.9 | 0.87 |
| 5 | transp, pr, incl | 0.0123 | 7 | 765 | 32.4 | 2.8 | 0.15 | 9154 | 0.04469 | 0.35 | 0.3232 | 0.40 | 0.05245 | 0.15 | 281.8 | 284.4 | 305.3 | 0.93 |
| 6 | flat-equant, euh | 0.0060 | 3 | 683 | 27.5 | 2.1 | 0.16 | 5233 | 0.04246 | 0.34 | 0.3026 | 0.41 | 0.05168 | 0.19 | 268.1 | 268.4 | 271.4 | 0.89 |
| 7 | lpr, clrls | 0.0018 | 1 | 563 | 24.4 | 2.9 | 0.41 | 969 | 0.04255 | 0.37 | 0.3038 | 0.73 | 0.05179 | 0.60 | 268.6 | 269.4 | 276.1 | 0.57 |
| 8 | eq brownish | 0.0035 | 1 | 416.5 | 26.3 | 1.4 | 0.64 | 3622 | 0.05784 | 0.39 | 0.4447 | 0.48 | 0.05576 | 0.28 | 362.5 | 373.5 | 442.8 | 0.81 |
| 9 | pink spr, tips | 0.0029 | 2 | 568 | 47.3 | 1.4 | 0.15 | 5718 | 0.07860 | 0.33 | 0.9549 | 0.38 | 0.08811 | 0.16 | 487.8 | 680.7 | 1385.0 | 0.91 |
| **Truzzo granite (TC5a)** | | | | | | | | | | | | | | | | | | |
| 10 | brown frags | 0.0073 | 1 | 349 | 29.2 | 32.8 | 0.22 | 430 | 0.08601 | 0.35 | 0.7106 | 0.80 | 0.05992 | 0.71 | 531.9 | 545.1 | 600.8 | 0.46 |
| 11 | lpr, clrls | 0.0036 | 3 | 1080 | 43.3 | 18.1 | 0.15 | 590 | 0.04240 | 0.34 | 0.3024 | 0.69 | 0.05172 | 0.56 | 267.7 | 268.2 | 273.1 | 0.59 |
| 12 | clear frags | 0.0076 | 2 | 595 | 32.6 | 9.1 | 0.17 | 1766 | 0.05707 | 0.34 | 0.4503 | 0.44 | 0.05724 | 0.24 | 357.8 | 377.5 | 500.6 | 0.85 |
| 13 | frags pr | 0.0075 | 2 | 759 | 34.5 | 2.0 | 0.17 | 8292 | 0.04778 | 0.36 | 0.3488 | 0.41 | 0.05294 | 0.19 | 300.9 | 303.8 | 326.2 | 0.89 |
| 14 | pr, clrls | 0.0063 | 2 | 561.7 | 26.6 | 15.1 | 0.11 | 751 | 0.05068 | 0.34 | 0.3750 | 0.60 | 0.05367 | 0.46 | 318.7 | 323.4 | 357.2 | 0.65 |
| 15 | lpr, clrls, incl | 0.0034 | 3 | 1294 | 51.0 | 6.1 | 0.09 | 1930 | 0.04248 | 0.33 | 0.3026 | 0.44 | 0.05166 | 0.24 | 268.2 | 268.4 | 270.5 | 0.84 |
| 16 | roundish frag | 0.0019 | 1 | 486 | 19.1 | 3.0 | 0.08 | 839 | 0.04242 | 0.41 | 0.3013 | 0.76 | 0.05151 | 0.63 | 267.8 | 267.4 | 263.9 | 0.56 |
| 17 | lpr, clrls | 0.0013 | 1 | 753.7 | 29.7 | 2.8 | 0.08 | 956 | 0.04246 | 0.34 | 0.3022 | 0.72 | 0.05161 | 0.59 | 268.1 | 268.1 | 268.0 | 0.58 |

a) euh = euhedral, clrls = colourless, incl = inclusions, pr = prisms; transp = transparent, frags = fragments; lpr = long prismatic, spr = short prismatic
b) Calculated on the basis of radiogenic $^{208}Pb/^{206}Pb$ ratios, assuming concordancy
c) Corrected for fractionation and spike
d) Corrected for fractionation, spike, blank and common lead (STACEY and KRAMERS, 1975)

to the average of the porphyric Truzzo granite and the Roffna rhyolite sets.

*Truzzo granite:* The zircon population is heterogeneous and typical for a crust-derived granite: Round to short-prismatic zircons of > 100 μm size have brown colour and often show resorption (pitted surface, rounded edges); inherited cores are visible through inclusions around them. Small short-prismatic pink zircons as well as long-prismatic colourless zircons are sharply faceted, with {211} faces dominating clearly over {110}. The zircons of this sample show a relatively large variation in measured U contents in zircon, up to a maximum of 1300 ppm U for long prismatic zircons representing inheritance-free, new growth in the melt. A discordia line defined by analyses 11, 12, 13, 14, 15 , 16 and 17 points to an upper intercept age of 505 ± 36 Ma, interpreted as an inherited age from a source rock. Analyses 10, pointing to an upper intercept age of 659 Ma, and 12 suggest that a second older component is present, too. The four analytically concordant points (11, 15, 16 and 17) cluster at a $^{206}Pb/^{238}U$ age of 268.0 ± 0.4 Ma, which agrees with the lower intercept age of 266.5 ± 4.5 Ma of a best-fit line calculated above.

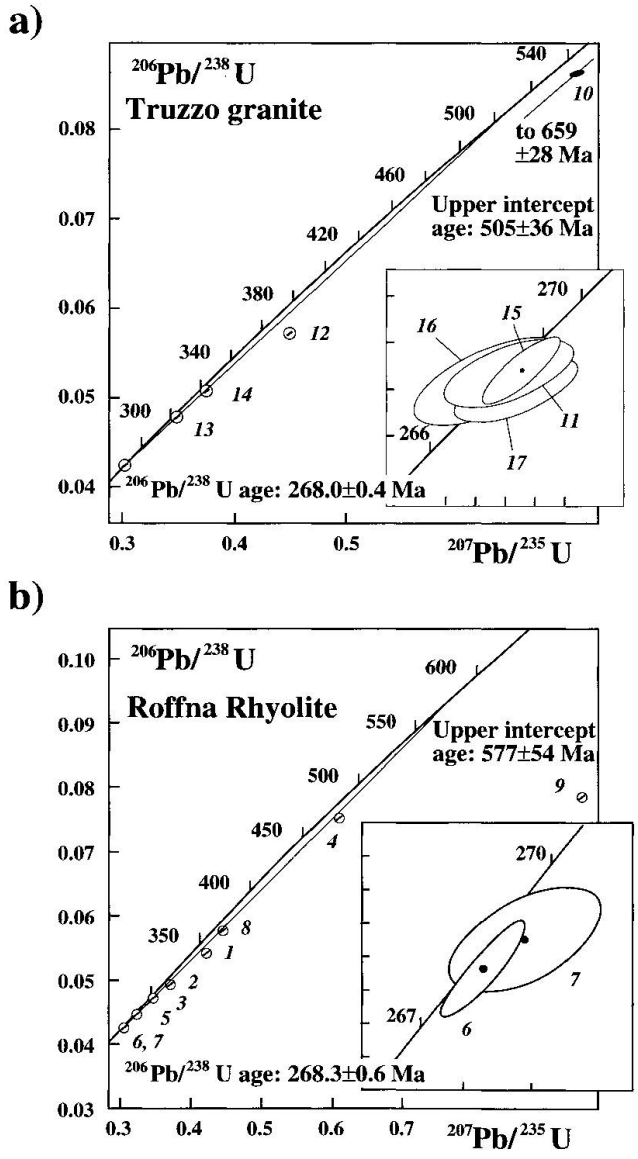


*Fig. 7* U–Pb diagrams for Truzzo granite (a) and Roffna rhyolite (b). Mean $^{206}Pb/^{238}U$ ages are at 95% confidence level.

*Roffna rhyolite:* The zircons of this sample show a similar morphology as those of the Truzzo granite. Short-prismatic zircons are brown to pink in colour and display visible cores through inclusions and turbidity. Prismatic to long-prismatic zircons show {211} as well as {110} faces, beside some very flat grains with {110} only. All zircons are nicely faceted and show no signs of resorption. The analyses show only a limited range of U concentration, despite a large variation in zircon morphology. Most of the analyzed grains or microfractions (2 to 8 grains) contain inherited lead from at least two sources. A best-fit line calculated with analyses 3, 5, 6 and 7 yield an upper intercept age of 577 ± 54 Ma, whereas analysis 9 (pointing to 2.0 Ga) suggests the presence of an additional component of Proterozoic age (Fig. 7b). The first age could possibly be a mixture between the two components of 505 and 659 Ma, respectively, found in the Truzzo granite. Only two analytical points plot near the concordia curve, at a mean $^{206}Pb/^{238}U$ age of 268.3 ± 0.6 Ma, with a slight offset towards higher $^{207}Pb/^{235}U$ values. Comparing these two points with the better constrained and more concordant points of the Truzzo granite (see above), we consider these two points as being concordant and their $^{206}Pb/^{238}U$ age therefore presents the best estimate for the age of zircon crystallization. A lower intercept age of 264.4 ± 3.4 Ma of a best fit line is calculated using analyses 3, 5, 6 and 7. It ranges within errors limits close to the above estimate $^{206}Pb/^{238}U$ age.

## Significance of Early Permian magmatism

Petrographical, geochemical and isotopic similarities suggest that the Truzzo granite and Roffna rhyolite are part of the same magmatic event. The analyzed Truzzo granite and Roffna rhyolite samples are representative of a number of small local intrusions in the Briançonnais basement and do not correspond closely in their geochemical compositions to magmas typical of the classical subduction cycle and related continental arc volcanism. The leucocratic granite samples and some samples of the porphyritic granite show charac-

teristics more typical of post-orogenic granites (Fig. 4, POG). The scattering of some of the Truzzo analyses, and the position of the Roffna rhyolite samples in the "Continental Collision Granitoids" field (Fig. 4, CCG) could be partly due to increased continental crust contamination and/or infracrustal melting, as is emphasised by the composition of the most contaminated sample HTC 7 located on the right part of the diagram (Fig. 4). The tectonic setting of these intrusions could be related to a post-orogenic event with the participation of crustal sources, as indicated by the occurrence of different types of xenoliths (BARBARIN and DIDIER, 1992). This strong crustal contamination is also emphasised by the results of the isotopic systems studies.

Both lithologies were derived from the same type of source and underwent similar magmatic processes. Knowing the geometry and the kinematics of the main Alpine deformations (BAUDIN et al., 1993; MARQUER et al., 1994, 1996) and the sedimentary records (STAMPFLI et al., 1998), it is possible to reconstruct the initial position of the Tambo and Suretta nappes before Alpine tectonics (Fig. 8A). The Truzzo granite and the Roffna rhyolite are closely located in the continental margin of the Briançonnais terrane in the Early Permian time, corresponding to two shallow but deep-rooted intrusions in the Briançonnais basement (Fig. 8). These intrusions appear as small plutons isolated in the old Briançonnais basement, as it was also described for other intrusions in the western Central Alps (e.g. Randa intrusion, Siviez-Michabel, THÉLIN et al., 1993), and differ from the large Variscan batholiths occurring in the External Crystalline Massifs. The acid magmatism was possibly triggered by mafic magmatism at the base of the crust (Fig. 8A: only one primary mag-

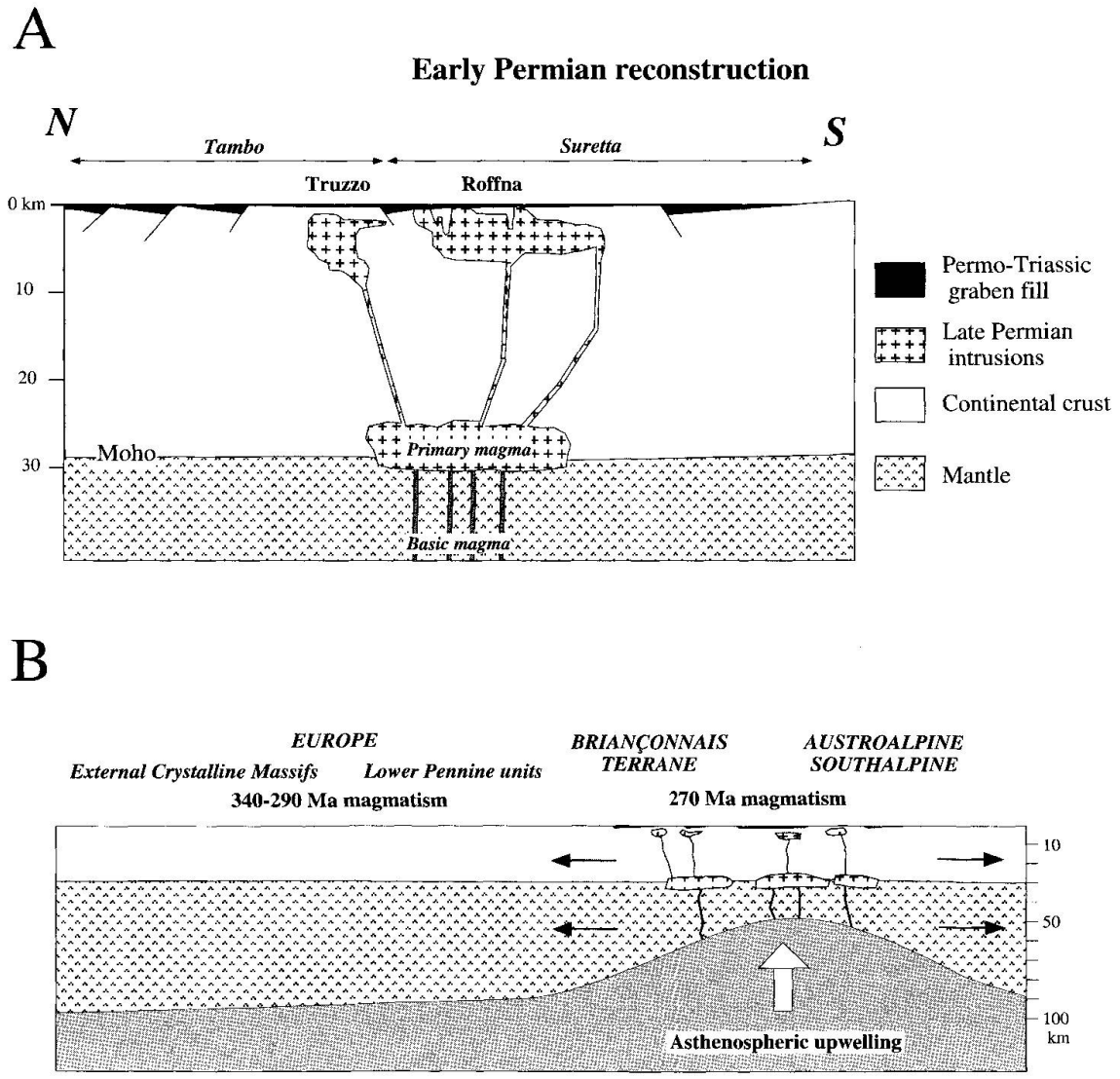


*Fig. 8* A Early Permian reconstruction of the Briançonnais continental crust with location of the Truzzo and Roffna granitoids. B: Schematic sketch of the tectonic setting of the Briançonnais domain during Early Permian time.

matic chamber is drawn), which led to partial melting of lower crustal sources, indicated by high initial Sr isotopic ratios and abundant inherited lead components in the dated zircons. The melts subsequently intruded into higher crustal levels and are currently found as cross-cutting Permian volcano-sedimentary sequences that were deposited in small sedimentary basins unconformably overlying the basement rocks (Fig. 8A).

The intrusion age of both Roffna and Truzzo protoliths can be dated around 268 Ma. The U–Pb system of zircon is thus less susceptible to effects of Alpine deformation and metamorphism than the Rb–Sr whole-rock systems. The age is similar to the U–Pb zircon date of 270 +6/–4 Ma from the nearby Braccia/Fedoz gabbro located at the boundary between Penninic and Austroalpine nappes (Margna nappe; HANSMANN et al., 1996) and to rhyolites and granites in Austroalpine, Penninic and Southalpine units, all scattering around 270–275 Ma (DEL MORO and NOTARPIETRO, 1987; STILLE and BULETTI, 1987; BARTH et al., 1994; BUSSY and CADOPPI, 1996; BUSSY et al., 1996). Large mafic complexes in the lower crust of the future southern margin of the Liguro-Piemontais ocean, such as the Braccia/Fedoz gabbro (Austroalpine-Malenco units, HERMANN et al., 1997) or in the Ivrea zone (Southalpine unit; HANDY and ZINGG, 1991; QUICK et al., 1994) demonstrate mafic underplating of this part of the crust. It is suggested that the upwelling of asthenospheric mantle below the Briançonnais and Austroalpine-Southalpine domains is responsible for the formation and emplacement of mafic intrusions during the Early Permian; the mantle melts in turn caused partial melting and granulitic metamorphism in the lower continental crust (DAL PIAZ, 1993; HERMANN, 1997). The strongly crust-contaminated melts rose into the upper crust and formed the Permian acid volcanism recorded in the Briançonnais and adjacent Austroalpine domains (Fig. 8B). Shallow-seated but possibly deep-rooted Early Permian intrusions are also described from more westerly areas of the Briançonnais terrane (e.g. Randa, Siviez-Michabel; THÉLIN et al., 1993).

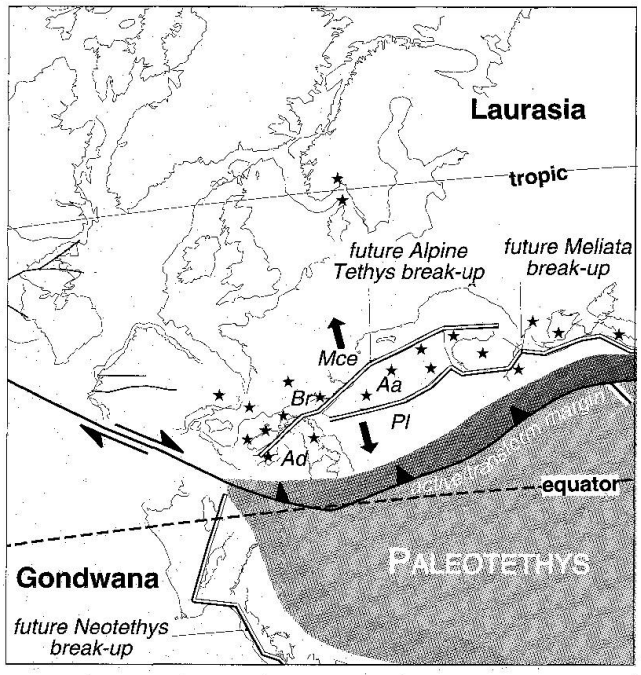


*Fig. 9* Early Permian framework of peri-Tethysian domains, modified after STAMPFLI et al. (1998). Aa: Austroalpine; Ad: Adria; Br: Briançonnais; Mce: External Crystalline Massifs; Pl: Pelagonia. Stars: Early Permian plutonism.

The Permian upwelling of the asthenosphere is thought to be caused by extensional plate tectonic forces leading to mega-shearzones concurrent with lithospheric thinning. The Early Permian extension is recorded by the volcano-sedimentary deposits in shallow basins at the top of the continental crust, mainly in the southern Penninic, Austroalpine and Southalpine domains (ZIEGLER, 1993). The type of Early Permian plutonism described here is found in a belt running from Catalonia (Spain), Corsica-Sardinia, Provence, Briançonnais, Southern Alps and Eastern Alps (see Fig. 9) and is different from the Visean to Stephanien magmatism widely exposed in the southern part of the Variscan orogen in Europe (BONIN et al., 1993; STAMPFLI, 1996). This latter, dominantly calk-alkaline magmatism is interpreted as related to subduction processes (FINGER and STEYRER, 1990; STAMPFLI, 1996) or as late- to post-orogenic magmatism related to post-convergence extension processes (BONIN et al., 1993; SCHALTEGGER and CORFU, 1995), for example in a basin-and-range-type setting (WERNICKE, 1992; GANS et al., 1989). The Briançonnais domain, however, seems to be lacking this Lower to Upper Carboniferous magmatism (Fig. 8B).

## Conclusions

Our new petrological investigations in the Truzzo granite and Roffna rhyolite of the central Alpine Briançonnais terrane show evidence for a magmatic event at 268 ± 1 Ma. An Early Permian reconstruction of the position of Truzzo granite and Roffna rhyolite in the Briançonnais terrane, based on the restoration of the Tertiary tectonics, emphasises the proximity of these intrusions. Both intrusions were shallow-seated and, as demonstrated here, are related to the same mag-

matic event. They might have their origin in upwelling asthenospheric mantle in Early Permian times, related to lithospheric thinning at the site of the future Jurassic rifting and opening of the Liguro-Piemontais ocean (DAL PIAZ, 1993; HERMANN, 1997).

Even if the upper intercept ages are poorly constrained in this study, the ages calculated from inheritance-bearing zircons of both lithologic units suggest the presence of different age components in the source or the contaminating host rocks (values around 2.0 Ga, 650 and 500 Ma). These values are typical of basement sequences in the Austroalpine, Penninic and Helvetic domains and in fact suggest that the composition of the basement in the Central Alpine segment is not significantly different from other basement parts of the Variscan orogen with respect to its pre-Carboniferous evolutionary history (SCHALTEGGER and GEBAUER, 1999). On the other hand, Early Permian magmatic activity is mainly restricted to the Briançonnais terranes and the Austroalpine-Southalpine units. It reflects a different setting than the late Variscan/Upper Carboniferous tectonic setting and related magmatism.

As a possible geodynamic scenario for this period we propose large shear zones running through the consolidated Variscan orogen, reaching deep into the lithosphere and causing lithospheric thinning, upwelling of asthenosphere and emplacement of mantle melts in the lower crust in Early Permian time.

## Acknowledgements

Financial support of the "Fonds National Suisse pour la Recherche Scientifique" (No 20-33421.92) is kindly acknowledged. We also thank H.R. Pfeifer (Lausanne) for XRF and J.J. Peucat (Rennes) for Rb–Sr analyses, as well as W. Wittwer for mineral separation and A. von Quadt for mass spectrometer maintenance at ETH Zürich. Reviews by F. von Blanckenburg, G. Schreurs, and M. Engi are gratefully acknowledged.

## References

BARBARIN, B. and DIDIER, J. (1992): Genesis and evolution of mafic microgranular enclaves through various types of interaction between coexisting felsic and mafic magmas. Transactions of the Royal Society of Edinburg: Earth Sciences, 83, 145–153.

BARTH, S., OBERLI, F. and MEIER, M. (1994): Th–Pb versus U–Pb isotope systematics in allanite from co-genetic rhyolite and granodiorite: implications for geochronology. Earth Planet. Sci. Lett., 124, 149–159.

BAUDIN, TH., MARQUER, D. and PERSOZ, F. (1993): Basement-cover relationships in the Tambo nappe (Central Alps, Switzerland): geometry, structures and kinematics. J. struct. Geol., 15, 3/5, 543–553.

BAUDIN, TH., MARQUER, D., BARFETY, J.C., KERCKHOVE, C. and PERSOZ, F. (1995): A new stratigraphical interpretation of the mesozoic cover of the Tambo and Suretta nappes: Evidence for early thin-skinned tectonics. C.R. Acad. Sci. Paris, t321, IIa, 401–408.

BIINO, G., MARQUER, D. and NUSSBAUM, CH. (1997): Alpine and Pre-Alpine subduction events in polycyclic basements of the Swiss Alps. Geology, 25/8, 751–754.

BLANC, B.L. (1965): Zur Geologie zwischen Madesimo und Chiavenna (Provinz Sondrio Italien). Mitt. Geol. Inst. ETH u. Univ. Zürich, 37.

BONIN, B., BRÄNDLEIN, P., BUSSY, F., DESMONS, J., EGGENBERGER, U., FINGER, F., GRAF, K., MARRO, CH., MERCOLLI, I., OBERHÄNSLI, R., PLOQUIN, A., QUADT, A. VON RAUMER, J.F. VON, SCHALTEGGER, U., STEYRER, H.P., VISONA, D. and VIVIER, G. (1993): Late Variscan magmatic evolution of the Alpine basement. In: VON RAUMER, J.F. and NEUBAUER, F. (eds): Pre-Mesozoic geology in the Alps. Springer-Verlag, Berlin Heidelberg, 171–201.

BUSSY, F. and CADOPPI, P. (1996): U–Pb zircon dating of granitoids from the Dora-Maira massif (western Italian Alps). Schweiz. Mineral. Petrogr. Mitt., 76, 217–233.

BUSSY, F., SARTORI, M. and THÉLIN, PH. (1996): U–Pb zircon dating in the middle Penninic basement of the Western Alps (Valais, Switzerland). Schweiz. Mineral. Petrogr. Mitt., 76, 81–84.

CHALLANDES, N. (1996): Déformation hétérogène et transferts de matière dans les zones de cisaillement des Roffna porphyres de la nappe de Suretta (Col du Splügen, Grisons). Diploma work, Neuchâtel.

COWARD, M. and DIETRICH, D. (1989): Alpine tectonics – an overview. In: COWARD, M.P., DIETRICH, D. and PARK, R.G. (eds): Alpine tectonics, Geol. Soc. Spec. Pub., 45, 1–29.

DALLA TORRE, M. (1991): Geologische und strukturgeologische Untersuchungen in des westlichen Val Ferrera (GR). Unpubl. Diplom thesis, Bern.

DAL PIAZ, G.V. (1993): Evolution of Austro-Alpine and Upper Penninic basement in the Northwestern Alps from Variscan Convergence to Post-Variscan Extension. In: VON RAUMER, J.F. and NEUBAUER, F. (eds): Pre-Mesozoic geology in the Alps. Springer-Verlag, Berlin Heidelberg, 327–344.

DEL MORO, A. and NOTARPIETRO, A. (1987): Rb–Sr Geochemistry of some Hercynian granitoids overprinted by eo-Alpine metamorphism in the Upper Valtellina, Central Alps. Schweiz. Mineral. Petrogr. Mitt., 67, 295–306.

FINGER, F. and STEYER, H.P. (1990): I type granitoids as indicators of a late Paleozoic convergent ocean continent margin along the southern flank of the central European Variscan orogen. Geology, 18, 1207–1210.

GANS, P.B., MAHOOD, G.A. and SCHERMER, E. (1989): Synextensional magmatismin the Basin and Range Province; A case study from the eastern great basin. Geol. Soc. Am. Spec. Pap., 233.

GANSSER, A. (1937): Der Nordrand der Tambodecke. Schweiz. Mineral. Petrogr. Mitt., 17/2, 291–523.

GRÜNENFELDER, M. (1956): Petrographie des Roffnakristallins in Mittelbünden und seine Eisenvererzung. Beitr. Geol. Karte Schweiz, 35, 57 pp.

GULSON, B.L. (1973): Age relations in the Bergell region of the South-East Swiss Alps: With some geochemical comparisons. Eclogae geol. Helv., 66/2, 293–313.

HANDY, M. and ZINGG, A. (1991): The tectonic and rheological evolution of an attenuated cross section of the continental crust: Ivrea section, southern Alps,

northern Italy and southern Switzerland. Geol. Soc. Am. Bull., 103, 236–253.

HANSMANN, W., HERMANN, J. and MÜNTENER, O. (1996): U–Pb-Datierungen an Zirkonen des Fedozer Gabbros, einer Intrusion an der Krusten-Mantel-Grenze. Schweiz. Mineral. Petrogr. Mitt., 76, 116–117.

HANSON, G.N., GRÜNENFELDER, M. and SOPTRAYNOVA, G. (1969): The geochronology of a recristallised tectonite in Switzerland – The Roffna gneiss. Earth and Planet. Sci. Lett., 5, 413–422.

HERMANN, J. (1997): The Braccia gabbro (Malenco, Alps): Permian intrusion at the crust to mantle interface and Jurassic exhumation during rifting. Ph. D. thesis, ETH-Zürich No. 12102., 194 pp.

HERMANN, J., MÜNTENER, O., TROMMSDORFF, V., HANSMANN, W. and PICARDO, G.B. (1997): Fossil crust-to-mantle transition, Val Malenco (Italian Alps). J. Geophys. Res., 102, B9, 20123–20132.

JÄGER, E., HUNZIKER, J.C. and GRAESER, S. (1969): Colloquium on the geochronology of Phanerozoic orogenic belts. Geochronology congress. Report and field trip guide book.

KROGH, T.E (1973): A low contamination method for the hydrothermal decomposition of zircon and extraction of U–Pb for isotopic age determinations. Geochim. Cosmochim. Acta 37, 637–649.

LA ROCHE, H. DE, LETERRIER, J., GRANCLAUDE, P. and MARSHAL, M. (1980): A classification of volcanic and plutonic rocks using R1-R2 diagram and major element analysis. Its relationships with current nomenclature. Chem. Geol., 29, 183–210.

LUDWIG, H.R. (1994): Isoplot: a plotting and regression for radiogenic isotope data. U.S. Geol. Surv. Open File Rep., 91–445, 43 pp.

MANIAR, P.D. and PICCOLI, P.M. (1989): Tectonic discrimination of granitoids. Geol. Soc. Amer. Bull., 101, 635–643.

MARQUER, D. (1989): Transfert de matière et déformation des granitoïdes – Aspects méthodologiques. Schweiz. Mineral. Petrogr. Mitt., 69, 13–33.

MARQUER, D. (1991): Structures et cinématique des déformations alpines dans le granite de Truzzo (Nappe de Tambo: Alpes centrales suisses). Eclogae geol. Helv., 84/1, 107–123.

MARQUER, D. and PEUCAT, J.J. (1994): Rb/Sr systematics of recrystallized shear zones at the greenschist-amphibolite transition: examples from granites in the Swiss Central Alps. Schweiz. Mineral. Petrogr. Mitt., 74/3, 343–358.

MARQUER, D., BAUDIN, TH., PEUCAT, J.J. and PERSOZ, F. (1994): Rb–Sr micas ages in the Alpine shear zones of the Truzzo granite: The timing of the Tertiary alpine P-T-deformations in the Tambo nappe (Central Alps, Switzerland). Eclogae geol. Helv., 87/1, 225–240.

MARQUER, D., CHALLANDES, N. and BAUDIN, TH. (1996): Shear zone patterns and strain partitioning at the scale of a Penninic nappe: the Suretta nappe (eastern Swiss Alps). J. Struct. Geol., 18/6, 753–764.

MILNES, A.G. and SCHMUTZ, H.U. (1978): Structure and history of the Suretta nappe (Pennine zone, Central Alps): A field study. Eclogae geol. Helv., 71/1, 19–33.

NUSSBAUM, CH., MARQUER, D. and BIINO, G. (1998): Two subduction events in a polycyclic basement: example of Alpine and pre-Alpine high pressure in the Alps (Suretta nappe, Swiss Eastern Alps). J. Metam. Geol. 16, 591–605.

PECCERILLO, A. and TAYLOR, R.S. (1976): Geochemistry of Eocene calk-alkaline volcanic rocks from the Kastamonu area, northern Turkey. Contrib. Mineral. Petrol., 58, 63–81.

PFIFFNER, O.A., FREI, W., VALASEK, P., STAUBLE, M., LEVATO, L., DUBOIS, L., SCHMID, S.M. and SMITHSON, S.B. (1990): Crustal shortening in the Alpine orogen: results from deep seismic reflection profiling in the eastern Swiss Alps line NFP 20-east. Tectonics, 9, 6, 1327–1355.

QUICK, J.E., SINIGOI, S. and MAYER, A. (1994): Emplacement dynamics of a large mafic intrusion in the lower crust, Ivrea-Verbano zone, northern Italy. J. Geophys. Res., 99, 21559–21573.

SCHAEREN, G. (1974): Geologisch-strukturelle Untersuchungen des unteren Val Madris und Val di Lei. Unpubl. Diploma thesis, ETH Zürich.

SCHALTEGGER, U. and GEBAUER. D. (1999): Pre-Alpine geochronology of the Central, Western and Southern Alps. Schweiz. Mineral. Petrogr. Mitt., 79/1, in press.

SCHALTEGGER, U. and CORFU, F. (1995): Late Variscan "basin and range" magmatism and tectonics in the Central Alps: evidence from U–Pb geochronology. Geodin. Acta, 8, 82–98.

SCHMID, S.M., RÜCK, P. and SCHREURS, G. (1990): The significance of the Schams nappes for the reconstruction of the paleotectonic and orogenic evolution of the Penninic zone along the NFP 20-East traverse (Grisons, Eastern Switzerland). Mém. Soc. Géol. Suisse, 1, 263–287.

SCHREURS, G. (1993): Structural analysis of the Schams nappes and adjacent tectonic units: implications for the orogenic evolution of the Penninic zone in the Eastern Switzerland. Bull. Soc. géol. France, 164, 3, 425–435.

STAMPFLI, G.M. (1996): The Intra-Alpine terrain: A Paleotethyan remnant in the Alpine Variscides. Eclogae geol. Helv., 89/1, 13–42.

STAMPFLI, G.M., MOSAR, J., FAVRE, PH., PILLEVUIT, A. and VANNAY, J.C. (1998): The Neotethys/East-Mediterranean basin connection. Peri-Tethys Memoir-IGCP, 369.

STAMPFLI, G.M., MOSAR, J., MARQUER, D. and MARCHAND, R. (1998): Subduction and obduction processes in the Swiss Alps. Tectonophysics (in press).

STACEY, J.S. and KRAMERS, J.D. (1975): Approximation of terrestrial lead isotope evolution by a two-stage model. Earth Planet. Sci. Lett., 26, 207–221.

STAUB, R. (1916): Zur Tektonik der Südöstlichen Schweizeralpen. Beitr. geol. Karte Schweiz (N.F.), 46. 198 pp.

STEINITZ, G. and JÄGER, E. (1981): Rb–Sr and K–Ar studies on rocks from the Suretta nappe; Eastern Switzerland. Schweiz. Mineral. Petrogr. Mitt., 61, 121–131.

STILLE, P. and BULETTI, M. (1987): Nd–Sr isotopic characteristics of the Lugano volcanic rocks and constraints on the continental crust formation in the South Alpine domain (N-Italy – Switzerland). Contrib. Mineral. Petrol., 96, 140–150.

STREIFF, V., JÄCKLI, H. and NEHER, J. (1976): Atlas géologique de la Suisse 1:25 000, 1235 Andeer, Comm. Géol. Suisse, 56.

STROHBACH, H. (1965): Der mittlere Abschnitt der Tambodecke samt seiner mesozoischen Unterlage und Bedeckung. Mitt. Geol. Inst. ETH u. Univ. Zürich, 38.

THÉLIN, P., SARTORI, M., BURRI, M., GOUFFON, Y. and CHESSEX, R. (1993): The pre-Alpine basement of the Briançonnais (Wallis, Switzerland). In: VON RAUMER, J. and NEUBAUER, F. (eds): The pre-Mesozoic geology in the Alps. Springer, Heidelberg, New-York, 297–315.

TRÜMPY, R. (1980): Geology of Switzerland, a guide

book. Part A: An outline of the geology of Switzerland. Schweiz. geol. Komm. Eds, Wepf Basel, 104 pp.
WEBER, W. (1966): Zur Geologie zwischen Chiavenna und Mesocco. Mitt. Geol. Ins. ETH u. Univ. Zürich, (N.F.), 57, 248 pp.
WERNICKE, B. (1992): Cenozoic extensional tectonics of the U.S. Cordillera. In: BURCHFIELD, B.C., LIPMAN, P.W. and ZOBACK, M.L. (eds): The geology of North America. Geol. Soc. Amer., G3, 553–581.
WILHELM, O. (1921): Geologische Karte der Landschaft Schams und Profile 1:50'000. Beitr. geol. Karte der Schweiz, Spezialk. 114A. Orell Füssli, Zürich.
WINCHESTER, J.A. and FLOYD, P.A. (1977): Geochemical discrimination of different magma series and their differentiation products using immobile elements. Chemical geology, 20, 325–343.
ZIEGLER, P.A. (1993): Late Palaeozoic–Early Mesozoic Plate Reorganization: Evolution and Demise of the Variscan Fold Belt. In: VON RAUMER, J. and NEUBAUER, F. (eds): The pre-Mesozoic geology in the Alps. Springer, Heidelberg, New York. 203–216.
ZURFLÜH, E. (1961): Zur Geologie des Monte Spluga. Mitt. geol. Inst. ETH u. Univ. Zürich, 83.

Manuscript received May 7, 1998; revision accepted September 14, 1998.

## APPENDIX

### ANALYTICAL TECHNIQUES

Rb–Sr: Rb and Sr contents were determined by XRF in the laboratory of Géosciences Rennes. Isotope analyses were also performed in Rennes using Cameca THN 206 and Finnigan Mat 262 mass spectrometers. The NBS 987 standard was measured at a value of $0.71020 \pm 5$ (internal error, $2\sigma$). Total error on the $^{87}Sr/^{86}Sr$ used in calculation is 0.025% (external error, $2\sigma$), although analytical errors were better ($3–8 \times 10^{-5}$ for THN206 measurements and $1–2 \times 10^{-5}$ for MAT262 measurements), for $^{87}Rb/^{86}Sr$ it is 1%. Isochrons were calculated according to the method of Ludwig (1994). The probable errors of the isochrons are quoted as $2\sigma \times \sqrt{MSWD}$, where MSWD > 1.

U–Pb: Conventional U–Pb analyses were carried out on microfractions or single zircons from a non-magnetic zircon fraction of a Frantz separator. Zircons were air-abraded to remove zones of marginal lead loss, washed in warm 4N nitric acid and rinsed several times with distilled water and acetone in an ultrasonic bath. Dissolution and chemical extraction of U and Pb were performed following KROGH (1973), using bombs and anion exchange columns that are scaled down to $^1/_{10}$ of their original size. Total procedural blanks were 2 pg Pb and 0.1 pg U. A mixed $^{205}Pb–^{235}U$ tracer solution was used for all analyses. Both Pb and U were loaded with Si-Gel and phosphoric acid on single Re filaments and measured on a Finnigan MAT 262 mass spectrometer using an ion counting system. The performance of the ion counter was controlled by repeated measurements of a NBS 982 standard solution.

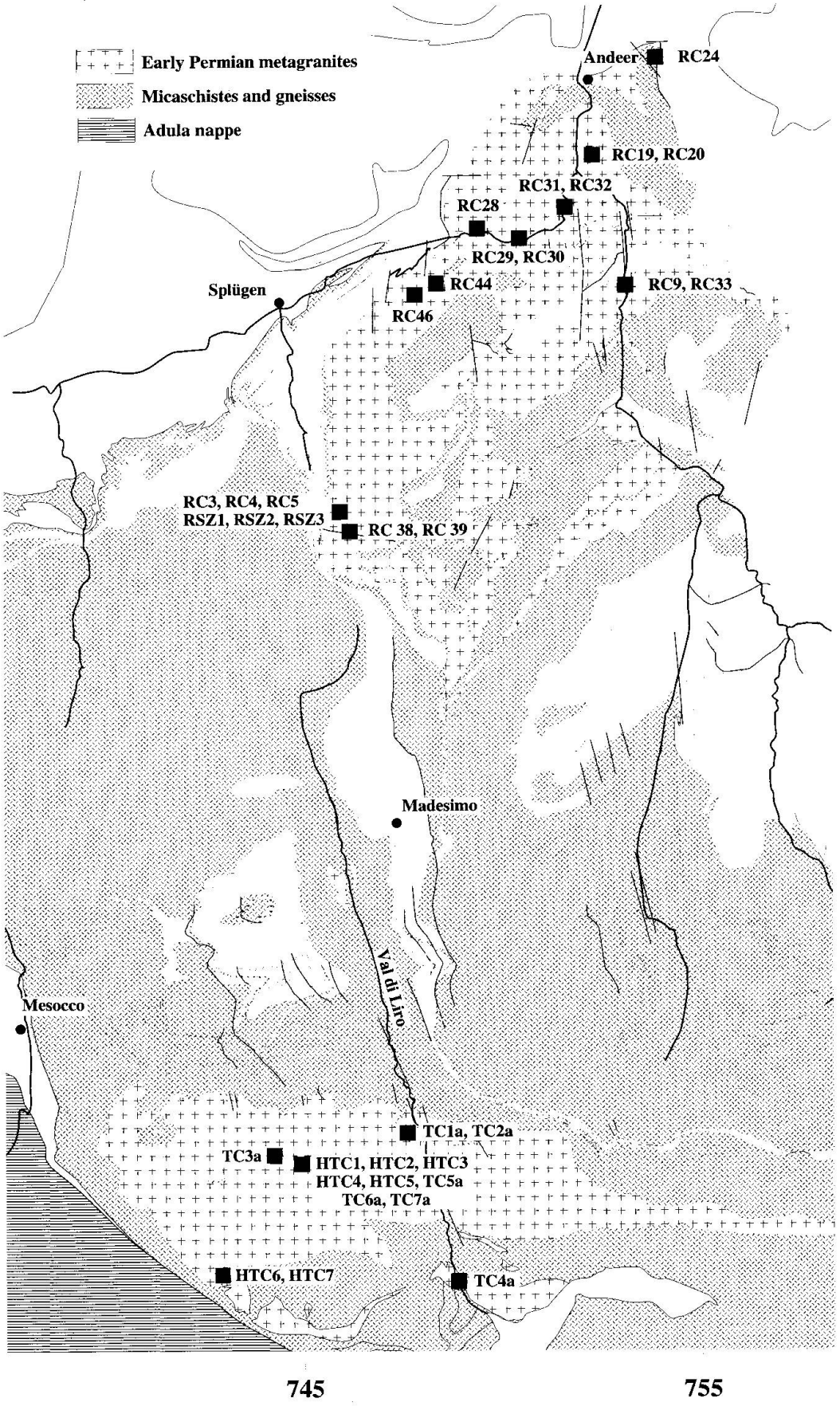


*Fig. 10* Locations of the samples analysed in the Truzzo granite and the Roffna rhyolite. See table 1 for detailed X-Y Swiss topographic coordinates.